Pharmaceutical Research, Vol. 23, No. 6, June 2006 (© 2006)
DOI: 10.1007/s11095-006-0142-8

Research Paper

FTIR and nDSC as Analytical Tools for High-Concentration Protein Formulations

Susanne Matheus,[1] Wolfgang Friess,[2] and Hanns-Christian Mahler[1,3,4]

Received November 10, 2005; accepted January 27, 2006

Purpose. The aim of the study is to evaluate Fourier-transform infrared spectroscopy (FTIR) as an analytical tool for high-concentrated protein formulations.
Methods. FTIR is used to determine the melting temperature ($T_{m\ (FTIR)}$) of various proteins, such as bovine serum albumin (BSA), immunoglobulin (IgG_1), β-lactoglobulin (β-LG), and lysozyme (HEWL), at different protein concentrations (5–100 mg/mL), where four data interpretation methods are discussed. The obtained $T_{m\ (FTIR)}$ values are further compared to the T_m measured by the nanodifferential scanning calorimetry (nDSC) technique.
Results. The $T_{m\ (FTIR)}$ values of IgG_1 and β-LG showed strong consistency and corresponded to the nDSC results irrespective of the method of data interpretation and the protein concentration applied. In contrast, the $T_{m\ (FTIR)}$ of BSA and HEWL is characterized by significant deviations. Only the midpoint of the second-derivative intensity–temperature curve of the intermolecular β-sheet mode measured at a concentration of 100 mg/mL is consistent with the nDSC results.
Conclusions. Determination of a $T_{m\ (FTIR)}$ is feasible by the midpoint of the intensity–temperature plot of the arising intermolecular β-sheet band. More significant results are obtained for proteins, which are predominantly composed of intramolecular β-sheet elements as well as at higher protein concentrations. A further study was started to assess the predictability of long-term protein stability by $T_{m\ (FTIR)}$.

KEY WORDS: DSC; formulation development; FTIR; high-concentration protein formulation; melting temperature.

INTRODUCTION

Because activities of the biotechnology industry were intensified in the early 1970s, the number of recombinant proteins—particularly of monoclonal antibodies—entering the therapeutic biologics market has been growing continuously. Currently, subcutaneous applicable protein products are preferred, particularly for the treatment of chronic diseases, requiring a limited injection volume of maximum 1–1.5 mL. Consecutively, the development of stable protein formulations at higher concentrations exceeding 100 mg/mL for monoclonal antibodies is necessary.

The main challenges during the designing and manufacturing of stable high-concentration protein formulations are basically well known from common protein therapeutics (1). Generally, formulation development focuses on the reduction of physical and chemical instability reactions and maintenance of the native, folded protein conformation (2–5). Nevertheless, additional considerations should be taken into account if dealing with highly concentrated protein therapeutics, which are, among others, the increased tendency to protein aggregation, a significant increase in viscosity, and the adaptation of analytical techniques to avoid potential artifacts during analysis (1,6).

The alteration of protein's native conformation is called denaturation, which is caused by a loss of protein tertiary and frequently secondary structure. The transition from the native state to a denatured state can either be a direct unfolding process or may pass through a series of partially or more extensively unfolded intermediate states leading to exposure of hydrophobic residues to the aqueous environment. The unfolded state can result in protein aggregation or may be more susceptible to protein degradation reactions (2–5,7,8). To ensure the integrity and stability of the native, folded structure of the protein, Volkin *et al.* (10) recommend the use of biophysical characterization methods to detect perturbations of the native structure, supported by biological assays to estimate the influence of unfolding on therapeutic function as well as thermodynamic techniques to gather information about the kinetics of the protein denaturation process. Different biophysical methods are available for the detection of unfolded protein molecules, such as spectroscopic techniques like near and far-ultraviolet (UV) absorption, intrinsic and extrinsic fluorescence, and near-UV circular dichroism (CD) spectroscopy to analyze the tertiary

[1] Merck KGaA, Global Pharmaceutical Development, Darmstadt, Germany.
[2] Department of Pharmacy, Pharmaceutical Technology and Biopharmaceutics, Ludwig-Maximilians-University Munich, Munich, Germany.
[3] Current address: F. Hoffmann-La Roche Ltd, Grenzacherstrasse 170, CH-4070 Basel, Switzerland.
[4] To whom correspondence should be addressed. (e-mail: Hanns-Christian.Mahler@roche.com)

protein structure as well as far-UV CD, Raman, and Fourier-transform infrared (FTIR) absorption spectroscopies to assess secondary structure. Other techniques used are optical rotatory dispersions, nuclear magnetic resonance, and viscosity measurements (9–11).

The advantages of the FTIR technique as compared to the other spectroscopic analytics are the small substance requirements, the rapid and easy use of the noninvasive technique, the lacking interference of buffer constituents and excipients (provided that a placebo solution identical to the protein sample is available), as well as the applicability to turbid liquids and different physical states of a sample (9,11–13). Thus, the use of FTIR analysis is reported in literature to evaluate changes in native secondary structure during lyophilization (14–20), spray drying (21,22), or manufacturing of particulate drug delivery systems (23,24), besides the exhaustive use of this technique for liquid protein samples to investigate protein folding and unfolding (25–28) or aggregation processes (17–31) and to elucidate qualitative and quantitative differences in the secondary structure composition (32,33). The application of FTIR analysis to monitor aggregation processes may be especially helpful in the formulation development of highly concentrated protein formulations. This is because of the fact that the increase in protein concentration leads to an increased packaging density and collision frequency fostering protein aggregation, because aggregation reaction kinetics are expected to be of second order or higher (2,34,35). Additionally, the formation of native, reversible self-association of protein molecules has to be taken into consideration for high-concentration proteins solutions as a result of the macromolecular crowding effects, i.e., the decrease in the effective volume because of the increased volume fraction occupied by the protein molecules (1). Furthermore, the FTIR technique could be exploited as a valuable tool in formulation development to identify suitable formulation conditions (pH, buffer system, stabilizing excipients, etc.) by quantifying either the overall similarity (20) or the area of overlap of two second-derivative spectra (36,37). Moreover, it is possible to determine a protein melting temperature (T_m), which is defined as the temperature at which equal amounts of native and denatured protein exist in equilibrium, as the midpoint of a spectroscopically measured transition, e.g., by monitoring the occurrence of amide I frequencies referred to denatured secondary structural elements as function of temperature (26,29,38,39).

Commonly, micro- or nanodifferential scanning calorimetry (μDSC or nDSC, with micro and nano describing the increase in sensitivity as compared to the standard DSC equipment) is used to determine the transition temperature T_m and to obtain data on the thermodynamics of protein folding and unfolding by measuring the excess heat capacity of a protein relative to buffer as a function of temperature (40). The observable parameters are T_m at the peak maximum, the enthalpy difference ΔH_m (calculated from the area under the C_p curve), and the heat capacity change ΔC_p for the transition between folded and denatured state of the protein. These parameters are directly related to the free energy change ΔG_u, which can be calculated by the Gibb–Helmholtz equation (38,40–42). μDSC/nDSC is increasingly used to identify the most stable protein mutant forms, to describe the unfolding process and its kinetics, to study the interaction of proteins with DNA, ligands, or ions, and—more importantly for formulation scientists—to detect and quantify the effects of potential stabilizing excipients on the melting temperature (43,44). Analytical methods applied in the designing and manufacturing of high-concentration protein formulations should avoid dilution of the protein solutions to measure the actual conditions and to prevent artifacts such as by potentially disturbing the protein's physical state (6). The concentration used in μDSC/nDSC analytics ranged from about 0.4 to 5 mg/mL to ensure that the effect of interactions between proteins is negligible and to avoid damage of the sample cells arising from the occurrence of precipitates favored at higher protein concentrations (45,46). This limitation is a major drawback of the method.

A suitable method for the determination of conformational stability of high-concentration protein samples used in formulation screening has to be economical with regard to the material requirements, quick and usable in a wide concentration range to avoid dilution of the samples, and maintain authentic measurement conditions. Because FTIR analysis is not restricted by an upper protein concentration limit—as it is the case for μDSC/nDSC measurements—and can be applied to elucidate protein conformational stability in the presence of different formulation conditions, there seems to be a great advantage of this technique for T_m determinations during the development of high-concentration formulations. However, the application of FTIR technique in this respect has not been published yet. A thorough cross-validation against the more straightforward thermoanalytical tool nDSC/μDSC, which is commonly used to obtain data on the thermodynamics of protein unfolding and enables assessment of different formulations on the basis of T_m values, has not been published previously but is deemed to be indispensable.

This study focuses on the evaluation of FTIR as analytical tool in the formulation development of high-concentration formulations. In the first part, FTIR was used to analyze the temperature-dependent unfolding behavior of four proteins (BSA, β-LG, HEWL, and a monoclonal antibody of the IgG_1 subclass) at different protein concentrations ranging from 5 to 100 mg/mL. The proteins were selected based on their different secondary structural elements (Table I). Four different interpretation methods to obtain a $T_{m\ (FTIR)}$ value are discussed. In the second part of this study, the measured $T_{m\ (FTIR)}$ values were compared with the data of the nDSC technique obtained by analysis of the highly concentrated protein formulations after performance of a dilution step.

MATERIALS AND METHODS

Materials

Four proteins were used to investigate the melting temperature with dependency on protein concentration and analytical method (FTIR, nDSC):

(a) bovine serum albumin (BSA, albumin fraction V from bovine serum; Merck KGaA, Darmstadt, Germany)

(b) a monoclonal antibody of the IgG_1 subclass (IgG_1, Merck KGaA)

Table I. Proteins Used and Their Characteristic Structural Data

	Protein	Molecular weight (kDa)	Secondary structure				
			α-Helix (%)	β-Sheets (%)	Turn (%)	Method	Reference
1	BSA	66.5	66.1	22.7	13.2	X-ray	(49)
2	IgG_1	153	3	67	18	X-ray	(53)
3	β-LG	17.5	6.8	51.2	9.9	X-ray	(58)
4	HEWL	14.6	41.1	9.3	35.7	X-ray	(42)

(c) β-lactoglobulin from bovine milk (β-LG, Fluka Chemie GmbH, Buchs, Switzerland)

(d) hen egg white lysozyme (HEWL, Fluka Chemie GmbH)

Sample Preparations

For FTIR measurements, each protein was formulated at a concentration of 5, 10, or 100 mg/mL in phosphate-buffered saline (PBS, pH 7.2) as a standardized formulation. PBS was prepared in water for injection, and its pH was adjusted to pH 7.2 with sodium hydroxide and hydrogen chloride solution. For nDSC measurements, each protein was diluted to a final concentration of 0.5, 2, and 5 mg/mL using PBS buffer (pH 7.2).

Analytical Methods

Fourier-Transform Infrared Spectroscopy

Infrared spectra of the protein solutions were recorded using a Tensor 27 spectrometer (Bruker Optik GmbH, Ettlingen, Germany). Protein samples were prepared in a BioATR (Attenuated Total Reflectance) cell™ II (Harrick), which is connected to a thermostat (DC30-K20, Thermo Haake). The BioATR sample cell can either analyze protein samples in solution or in suspension. For each spectrum, a 128-scan interferogram was collected at a single beam mode with a 4-cm^{-1} resolution. Reference spectra were recorded under identical conditions with only the reference buffer in the cell. To determine the melting temperature ($T_{m\ (FTIR)}$) of the four proteins, temperature-dependent spectra were acquired at three different concentrations (5, 10, and 100 mg/mL) every 2°C for the following temperature ranges: 40–80°C for BSA and 60–90°C for the IgG_1 antibody, β-LG, and HEWL. The temperature ranges were identified in previous studies (data not shown). Recorded infrared spectra were analyzed by the software Protein Dynamics for Opus 4.2 (Bruker Optik GmbH) and displayed as vector-normalized second-derivative amide I spectra [calculated with 25 smoothing points according to the Savitzky-Golay algorithms (48)].

Nanodifferential Scanning Calorimetry

Calorimetric measurements were performed on a CSC Model 6300 Nano III differential scanning calorimeter (Calorimetry Sciences Corp, Lindon, UT, USA) using the DscRun software. Scanning calorimetry was performed for each model protein at three concentrations (0.5, 2, and 5 mg/mL), employing a heating rate of Δ = 1°C/min for a temperature range from 25 to 110°C. The protein solution was filled into the sample cell, the reference buffer in the reference cell, and a constant pressure of 3 atm was applied. Buffer–buffer tracings were recorded under the same conditions and subtracted from the sample endotherms. Subsequently, curve analysis using the converter object of the CpCalc software led to the excess heat capacity curve offering information about the melting temperature ($T_{m\ (nDSC)}$) as well as the calorimetric enthalpy (ΔH_m) and entropy (ΔS_m) of the unfolding process normalized for protein concentration.

RESULTS AND DISCUSSION

FTIR Spectra and Temperature-Induced Structural Changes of the Four Proteins

The FTIR spectrum of proteins can be distinguished in nine protein-sensitive amide bands, called A, B, and I–VII, which, in general, result from the absorption of energy by vibration of the amide backbone linkage. Because the primary components of the amide I band ranging from 1700 to 1600 cm^{-1} are mainly generated by C=O stretching vibrations, the band is influenced by hydrogen bonding, and thus, information about conformational changes are provided (11,12,17). A second-derivative procedure is used to resolve the overlapping secondary structural elements contributing to the amide I band, whereby the band position is preserved (12,48). Table II shows the assignment of the principal amide I frequencies to the protein secondary structure as previously described in the literature (11,12).

By increasing the temperature during FTIR analysis of the four model proteins, perturbations in secondary structures occurred, resulting in changes of the respective secondary structural amide I mode (Fig. 1). Starting the temperature ramp, BSA (Fig. 1a) exhibited the amide I band maximum at 1656 cm^{-1}, a frequency characteristic to

Table II. Assignment of Amide I Component Frequencies to Protein Secondary Structure Elements [According to (12,48)]

Frequency (cm^{-1})	Assignment
1612–1642 (strong)	Intramolecular β-sheet
1670–1690 (weak)	
1615–1625	Extended strand (intermolecular β-sheet)
1640–1651	Unordered (random coil)
1650–1657	α-Helix
1655–1675	Turn
1680–1696	

proteins containing predominantly α-helical structures. Besides that, assignment of frequencies centered around 1630 cm^{-1} to extended chains that connect helical cylinders and of the amide I mode around 1670 cm^{-1} to β-turns is feasible. This is in good agreement with data obtained by X-ray diffraction analysis confirming albumin to be mainly an α-helical protein (49) as well as with other FTIR studies of human serum albumin (31,50,51). Elevation of temperature up to 80°C resulted in spectral changes as follows: the amide I absorbance maximum near 1656 cm^{-1} decreased as a function of temperature, accompanied by an intensity increase at 1622 cm^{-1}. According to the results of Militello *et al.* (32), who suggested that the heat-induced aggregation process of BSA at a pH value far away from the isoelectric point of the protein (pH 7.4) proceeds prevalently in an ordered way to form β-aggregates, frequencies assignable to unordered structures could not be monitored, whereas the occurrence of random coil structures in BSA solution is described for lower pH values (pH 6.2).

Heating the IgG_1 antibody solution from 60 to 90°C also resulted in a drastic change in the contour of the amide I band (Fig. 1b). The main frequencies of the native FTIR spectrum can be assigned as follows: the bands at 1689 and 1639 cm^{-1} could be attributed to β-sheets, the peaks at 1676 and 1663 cm^{-1} to turns, and the mode at 1616 cm^{-1} either to β-sheets or to side-chain effects (21,52). The main contribution of β-sheet structure to the secondary structure of the IgG_1 antibody corresponds to the data of X-ray analysis (53). With increasing temperature, a shift to a strong temperature-induced frequency at 1625 cm^{-1} and a weak intensity peak at 1695 cm^{-1} at the expense of the band at 1639 and 1689 cm^{-1} that are assignable to intramolecular β-sheets became obvious.

Looking at the spectrum of β-LG (Fig. 1c) recorded at the beginning of the temperature profile, the amide I contour could be resolved in the following components according to previous studies described in literature: the bands at 1690 and 1630 cm^{-1} are a result of antiparallel β-sheets, the frequency at 1656 cm^{-1} is caused by α-helix, the modes at 1681, 1667, and 1661 cm^{-1} are caused by turns, and the peak at 1646 cm^{-1} is caused by unordered structures (33,54–56). The intensity of the main peak centered at 1630 cm^{-1} assignable to intramolecular β-sheet structural elements was diminishing when applying a temperature ramp ranging from 60 to 90°C. Concomitant with this decrease at 1630 cm^{-1} was a strong increase in spectral intensity at 1621 cm^{-1} and a slight one at 1695 cm^{-1}. Structural changes in the α-helical mode at 1656 cm^{-1} were less prevalent because β-LG is composed of a significantly higher β-sheet content in comparison to α-helix as shown by X-ray and FTIR analysis (57,58). Additionally, slight structural perturbations could be detected in the increasing intensity of the band at 1645 cm^{-1} originating from random coil structures.

Figure 1d shows the infrared spectra of HEWL recorded at various temperatures. At the beginning of the temperature

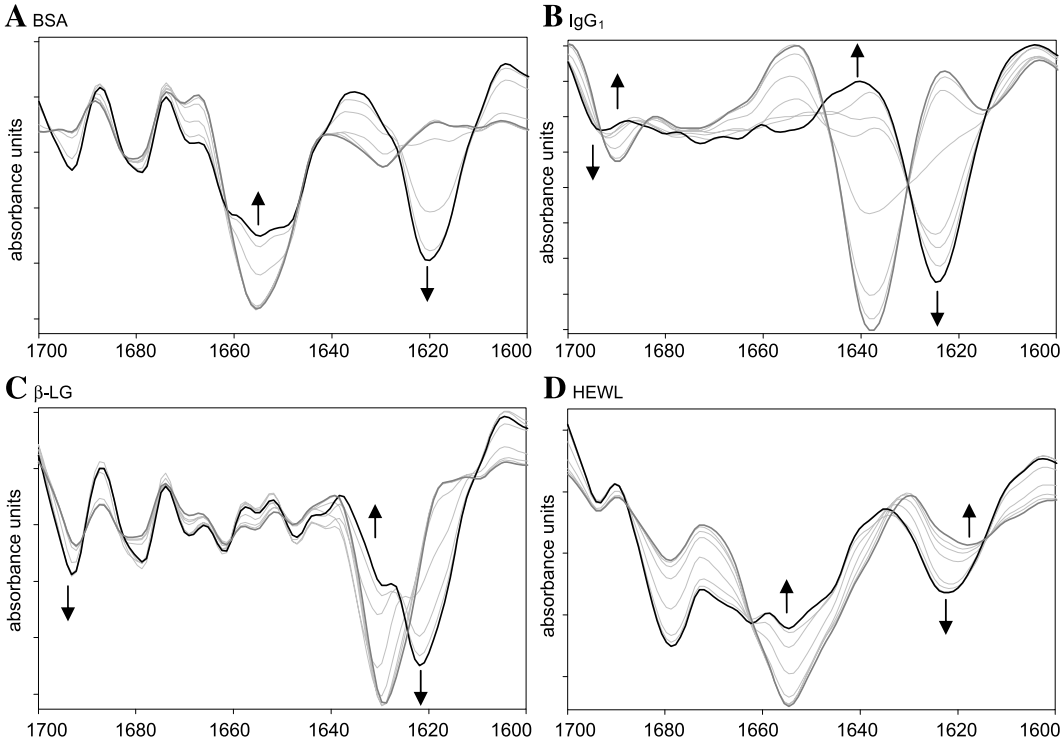

Fig. 1. Second-derivative, vector-normalized amide I spectra of (A) bovine serum albumin (BSA), (B) IgG_1 antibody, (C) β-lactoglobulin (β-LG), and (D) HEWL each formulated at a concentration of 100 mg/mL in phosphate-buffered saline (PBS), pH 7.2. The temperature-dependent recording of the spectra was performed according to the conditions described in Materials and Methods with the gray and the black bold lines showing the spectrum at the beginning or the end of the temperature ramp, respectively. The intermediate spectra are displayed as thin lines. For reasons of clarity, only the spectra recorded at intervals of 4°C (IgG_1, β-LG, and HEWL) or 6°C (BSA) are shown. The arrows indicate the direction of spectral changes.

ramp, the FTIR spectrum showed an absorbance maximum at 1656 cm^{-1} indicating a predominantly α-helical structure. This result is consistent with those reported by X-ray crystallographic analysis (42) and further FTIR investigations (57). Besides the peak at 1680 cm^{-1} originating from turn structures, the smaller contribution of the β-sheets to the secondary structure could be reflected by the bands at 1619 and 1695 cm^{-1} and the shoulder at 1642 cm^{-1} (12,59). As temperature increases, a novel band arose at 1623 cm^{-1}. Correspondingly, the occurrence of a band at 1615 cm^{-1}, which is attributed to the native HEWL secondary structure, and of a band at 1628 cm^{-1} appearing in heat-denatured samples is described by van de Weert *et al.* (38). The authors assumed that these bands do not necessarily originate form the same structural element.

The thermal unfolding of all investigated proteins was characterized by appearance of a strong low-frequency band around 1620–1625 cm^{-1}, which originates from the formation of intermolecular hydrogen-bonded antiparallel β-sheet structures at the expense of other regular structures. A weaker high-frequency band around 1695 cm^{-1} becomes apparent, especially in the spectra of β-LG and the IgG_1 antibody, and can be also associated with intermolecular β-sheet formation (5,17,60). In addition to the appearance of infrared amide I bands assigned to intermolecular β-sheets, the presence of new protein interactions after heating was documented by the observation of gel formation of the cooled samples, which are characteristic for extensive intermolecular interactions in protein samples (29). However, for the α-helical proteins BSA and HEWL, the bands indicative of intermolecular β-sheet formation do not appear in such significant intensity as they could be monitored in the temperature-induced spectra of β-LG and the IgG_1 antibody, in which secondary structure is dominated by intramolecular β-sheets. In the spectra recorded for HEWL at a lower protein concentration (5 and 10 mg/mL), the peak attributed to intermolecular β-sheet aggregates is hardly detectable at all at 90°C (Fig. 2). Instead, the absorbance maxima of the native spectrum at 1656 and 1619 cm^{-1} shifted toward a peak centered around 1650 cm^{-1} resulting in a broadening of this peak and pointing to the formation of random coils. Although it is difficult to distinguish the unordered from the α-helical component in nondeuterated samples, this secondary structural element can appear as an asymmetric shoulder on the low-frequency side of the α-helix band (12,48). This is in good agreement with the results of Dong *et al.* (30), who reported that the thermally perturbed state of a 40-mg/mL aqueous HEWL solution contains only a negligible amount of β-sheet aggregates, but is represented by two broad bands at 1657 and 1685 cm^{-1}, assignable to the residual α-helix and β-turn structure, respectively. A comparable mechanism was observed for the amyloid formation of p53 tetramerization domain by Lee *et al.* (61). FTIR spectroscopy was used to confirm the temperature-induced structural transition of the tetramerization domain of the wild-type p53 proceeding from the native α-helical conformer via a denatured state composed of random peptide conformation to a stable intermolecular β-strand rich conformation. The higher protein concentration of 100 mg/mL HEWL used in this study seems to enable the formation of β-sheet aggregates at a detectable amount

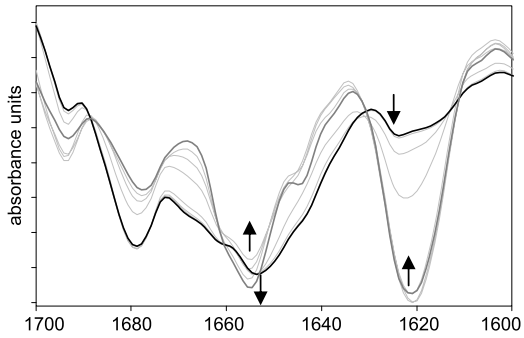

Fig. 2. Second-derivative, vector-normalized amide I spectra of HEWL at a concentration of 5 mg/mL in PBS, pH 7.2, recorded as a function of temperature. The temperature-dependent recording of the spectra was performed according to the conditions described in Materials and Methods with the gray and the black bold lines showing the spectrum at the beginning or the end of the temperature ramp, respectively. The intermediate spectra are displayed as thin lines. For reasons of clarity, only the spectra recorded at intervals of 4°C are shown. The arrows indicate the direction of spectral changes.

(Fig. 1d) because the aggregation process is fostered by protein concentration as a result of its second or higher reaction order (2,34,35). Generally, noncovalent protein aggregation involves mostly intramolecular β-sheets, whereas α-helix structures seem to be less likely to form aggregates. This may be caused by a stronger dipole moment of α-helices as compared to that of the β-sheets (62).

Determination of $T_{m\ (FTIR)}$ of the Four Proteins

Thermally induced structural transitions in the secondary structure monitored by recording the infrared spectra as a function of temperature are described in literature (26,29, 38,39) to analyze the unfolding behavior of proteins and to determine a melting temperature ($T_{m\ (FTIR)}$). Because the structural transition to intermolecular β-sheets occurs regardless of the initial secondary structure composition of the native protein, these bands can be used to monitor denaturation and aggregation reactions in both aqueous and solid state (4). Cauchy *et al.* (40) plotted the fraction of denatured recombinant human growth hormone *vs.* temperature to obtain the thermal transition temperature as midpoint of the thermal denaturation curve and to calculate the free energy (ΔG_u) and enthalpy (ΔH_u) of protein unfolding. The protein unfolded fraction (f_u) was calculated by use of the peak height of an amide I frequency at 1620 cm^{-1}, which can be related to intermolecular β-sheet formation, and is based on an equation used by Pace *et al.* (11) for the analysis of protein unfolding curves. Otherwise, direct plots of the intensity values, either of the decreasing native amide I mode or of the arising temperature-induced structural frequency, have been applied to gain the onset as well as the midpoint of the thermal transitions of recombinant human factor XIII (26), of the α-helical proteins myoglobin, cytochrome *c*, and lysozyme (29), and of recombinant human interferon-γ (63). The intensity ratio of the amide I band at 1616 and 1650 cm^{-1} was used as an indicator of the thermal unfolding of cytochrome *c* and to determine the midpoint denaturation temperature (64). In addition to literature, the point of cross

section between the temperature-dependent intensities of the temperature-induced frequency with the disappearing amide I mode is another possible analysis tool.

In this study, four different data interpretation methods to extract the melting temperature ($T_{m\ (FTIR)}$) were evaluated. The approaches used are shown exemplary in Fig. 3 for the thermal unfolding of the IgG_1 antibody at a concentration of 100 mg/mL (Fig. 1b). The transition temperature ($T_{m\ (FTIR)}$) was obtained by calculation of the midpoint of the thermal denaturation curves by use of the Microcal™ Origin™ software (version 5.0, Microcal Software Inc., Northampton, MA, USA) and applying a sigmoid fit according to the Boltzmann model. The thermal transition curves were received by plotting the intensities of the following frequencies *vs.* the temperature: the intensity of the increasing ("temperature-induced structural element") band of the vector-normalized second-derivative amide I spectrum (method i; Fig. 3a); the intensity of the decreasing ("structural loss") band of the vector-normalized second-derivative amide I spectrum (method ii; Fig. 3b); and the ratio of the intensities of the arising to the vanishing band of the nonmodified amide I spectrum (method iii; Fig. 3c). Furthermore, the point of cross section between the increasing and decreasing band of the vector-normalized second-derivative amide I spectrum could be determined (method iv; Fig. 3d) as the $T_{m\ (FTIR)}$ value.

Table III summarizes the $T_{m\ (FTIR)}$ values for BSA, β-LG, HEWL, and the IgG_1 antibody in dependency on protein concentration, with the results of the sigmoid fitting procedures being listed with the standard deviation. The results obtained for the proteins with a high intramolecular β-sheet content (i.e., IgG_1, β-LG) show a strong consistency in the obtained numeric values for $T_{m\ (FTIR)}$, irrespective of the method of data interpretation and the protein concentration applied. In contrast, the values of the α-helical proteins are characterized by significant deviations. The $T_{m\ (FTIR)}$ values of BSA originating from the midpoint of the ratio of the increasing to the decreasing band as well as of the intensity of the structural loss band in the second derivation were only applicable at 100 mg/mL or 10 and 100 mg/mL, respectively. For both BSA and HEWL, differences of approximately 7°C in the $T_{m\ (FTIR)}$ values resulted from calculations based on the midpoint of the intensity of the intermolecular β-sheet structures in the second-derivative spectrum. Using the midpoint of the intensity–temperature curve of the α-helix mode for HEWL resulted in large deviations of the $T_{m\ (FTIR)}$ values in the range of 20°C. This can be attributed to the differences in the FTIR spectra of HEWL at different concentrations (Figs. 1d and 2). Explicitly, the broadening of the α-helix band at the lower concentration range accompanied with the appearance of a shoulder at 1650 cm^{-1} led to an improper "S"-shaped curve making sigmoid fitting very

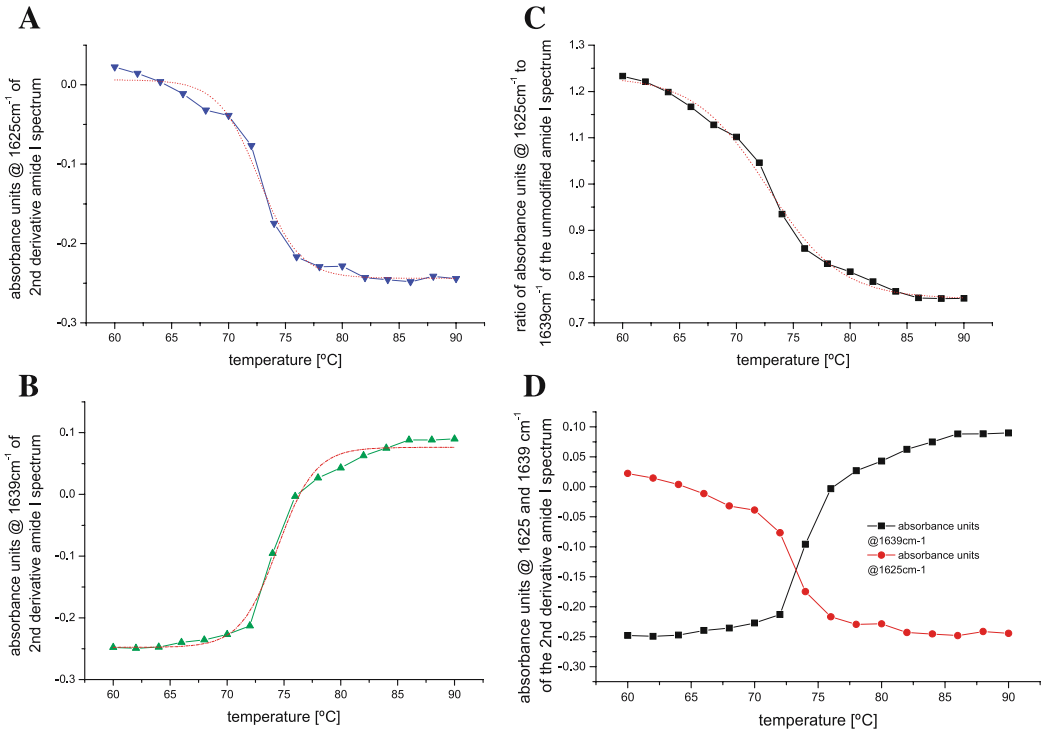

Fig. 3. $T_{m\ (FTIR)}$ interpretation methods of thermal transition curves (solid lines) of the IgG_1 antibody obtained by sigmoidal fittings (dotted lines) of the plotting of (A) method i: intensity of the thermally induced increasing second-derivative infrared amide I band; (B) method ii: the intensity of the decreasing second-derivative infrared amide I band; (C) method iii: the ratio of the intensities of the increasing to the decreasing nonmodified amide I band *vs.* temperature; or by (D) method iv: determination of the point of cross section between the intensities–temperature curves of the increasing to the decreasing second-derivative amide I band. The data interpretation approaches are shown exemplary for the IgG_1 antibody formulated at a concentration of 100 mg/mL in PBS, pH 7.2.

Table III. Transition Temperatures ($T_{m\,(FTIR)}$) of Four Proteins with Dependency from Protein Concentration Obtained by Different Data Interpretation Methods of FTIR Results

		$T_{m\,(FTIR)}$ (°C), obtained with different calculation models			
		Midpoints			
Protein	Concentration (mg/mL)	Method i: increasing band (second derivation)	Method ii: decreasing band (second derivation)	Method iii: ratio of increasing to decreasing band	Method iv: point of cross-section between increasing and decreasing band
BSA	5	74.5 ± 1.9	n.a.[a]	n.a.[a]	n.a.[a]
	10	70.8 ± 1.1	67.8 ± 0.5	n.a.[a]	n.a.[a]
	100	68.6 ± 0.2	71.3 ± 0.3	66.8 ± 0.2	n.a.[a]
IgG_1	5	74.3 ± 0.2	76.3 ± 0.5	73.8 ± 0.3	75.0
	10	73.3 ± 0.1	75.2 ± 0.3	73.6 ± 0.3	74.0
	100	74.7 ± 0.1	76.1 ± 0.3	74.3 ± 0.2	75.3
β-LG	5	82.0 ± 0.6	81.6 ± 1.0	81.6 ± 0.5	80.1
	10	79.9 ± 0.7	78.1 ± 0.7	80.2 ± 0.9	80.4
	100	79.8 ± 0.2	79.6 ± 0.1	80.1 ± 0.3	81.2
HEWL	5	79.5 ± 0.3	61.1 ± 0.9	79.1 ± 0.3	n.a.[a]
	10	79.4 ± 0.6	60.5 ± 1.2	78.9 ± 0.4	n.a.[a]
	100	74.3 ± 0.5	78.6 ± 0.2	75.3 ± 0.3	n.a.[a]

FTIR = Fourier-transform infrared spectroscopy.
[a] n.a. = not applicable or detectable (see text).

challenging. Furthermore, the increased formation of β-sheet aggregates at the higher concentration could explain the decreased $T_{m\,(FTIR)}$ values originated from the intensity–temperature plot of the intramolecular β-sheet structure. The interpretation of FTIR data using the point of cross section between the intensities of the α-helical mode with the temperature-induced structural mode at about 1620 cm^{-1} could not be applied for BSA and HEWL because the intensity increase caused by intermolecular β-sheets was significantly smaller than the decrease of the native α-helix mode. Overall, complications in the data interpretation methods of proteins composed predominately of α-helical structural elements seem to be a result of the fact that those proteins are less prone to the formation of β-sheet aggregates as compared to intramolecular β-sheets because of the stronger dipole moment of α-helices (62).

Slight differences in the $T_{m\,(FTIR)}$ values were also observed for the proteins mainly composed of β-sheets. The $T_{m\,(FTIR)}$ of the IgG_1 antibody increases in the following order according to the method of data interpretation applied: midpoint of the second-derivative intensity of the temperature-induced structure (method i) ≤ midpoint of the ratio of the intensities of the arising to the vanishing band using the nonmodified amide I spectrum (method iii) < point of cross section between the intensities of the native and denatured frequencies in the second-derivative spectrum (method iv) < midpoint of the second-derivative intensity of the structural loss band (method ii). The differences in the transition temperatures with reference to a distinct secondary structural element are in contradiction to the results of Moritz *et al.* (28), who stated a coincidence in the temperature profiles of a wild-type RNase T1 and its variant independent from the selection of the amide I band. The $T_{m\,(FTIR)}$ values were derived from different spectral components comprising, on the one hand, arising structures and, on the other hand, vanishing structures. The authors suggested a highly cooperative two-state unfolding and refolding process for both proteins under equilibrium conditions. Although the calculation of the β-LG $T_{m\,(FTIR)}$ values based on the main diminishing band (intramolecular β-sheets) as well as on the temperature-induced amide I mode (intermolecular β-aggregates) revealed only minor deviations, the transition temperature of the other structural component, the α-helix, is significantly lower (73.9 ± 0.6°C; data not shown). Likewise, Hoffmann *et al.* (65) noticed an asymmetrical peak in DSC analysis with a left-side shoulder at lower temperatures by use of a very low scan rate of 2°C/h. Moreover, a minor $T_{m\,(FTIR)}$ value of BSA was discerned, if it was referred to the intensity–temperature curve of a short segment chain connecting the α-helical segments instead of using the bands assignable to the α-helix, turn, and intermolecular β-sheet structures (50).

Looking at the complete data set of the four proteins, the results could not be correlated to protein concentration. Because of the lack of possibility to utilize all data interpretation methods for the α-helical proteins over the total concentration range, the use of high concentrations (preferentially above 10 mg/mL) is recommended for determination of the T_m using FTIR. In fact, many FTIR studies are conducted at a protein concentration ranging from 20 to 60 mg/mL (21,29,31,37,50,51,57). An increase in protein concentration could possibly favor aggregation processes—as it is the case for lysozyme, but results in a better signal-to-noise ratio. This is especially important, if a data interpretation method using the second-derivative spectra is applied, because the major problem in derivative spectroscopy is the rapid decrement of the signal-to-noise ratio as the order of the derivative increases. The derivation procedure amplifies disproportionably the weak features in the spectrum, originating from random noise and uncompensated water vapor (48). Thus, the absence of any of the described artifacts in the region where no infrared bands due to functional groups are

expected (e.g., between 1750 and 1850 cm^{-1}) should be verified. Smoothing could be applied to reduce noise fluctuations, but the possibility for the introduction of distortion into the FTIR spectra should be kept in mind (47). Hence, the importance of high-quality infrared spectra (preferably with a signal-to-noise ratio better than 500:1) can never be overemphasized and is favored by the use of high protein concentrations (48). Besides that, the availability of a well-formed sigmoid intensity–temperature plot with an unambiguous pre- and posttransitional baseline is an essential prerequisite for the application of the Boltzmann fit (42). The best fit can be estimated by the standard deviation of the fitted parameters and the chi-square value.

The use of signal–temperature curves in contrast to curves plotting the fraction unfolded (39) does not allow the derivation of thermodynamic parameters. Nevertheless, for such thermodynamic interpretation, it is of utmost importance that the unfolding reaction is reversible and has reached equilibrium at the time of measurement. Irreversibility is frequently observed with multidomain proteins where the domains unfold independently, but may also occur in case of a single-step unfolding (10). It can result from a number of covalent and conformational changes, e.g., aggregation, formation, destruction or scrambling of disulfide bonds, deamidation, and hydrolysis (35,66). Another disadvantage coming along with spectroscopic techniques is the lack of direct measurement of intermediates in the unfolding process (42) and, at the same time, the fact that in most solution conditions—especially at protein concentrations exceeding 2 mg/mL—available intermolecular interactions do not allow application of a simple thermodynamic two-state model (67). Because the proteins used in this study are, without exceptions, multidomain proteins and the concentration range of interest is 100 mg/mL, it is not recommended to use FTIR analysis for thermodynamic investigations of such.

Determination of $T_{m\ (nDSC)}$ of the Four Proteins

Nanodifferential scanning calorimetry was used in this study to cross-check the transition temperatures obtained by infrared spectroscopy. This includes the identification of a suitable FTIR data interpretation method that fits the $T_{m\ (nDSC)}$ values best and is applicable reliably over a wide range of differentially composed proteins, especially for measurements at higher protein concentrations (≥100 mg/mL). Because the nDSC technique requires low protein concentrations to avoid precipitation, thus preventing mechanical damaging of the sample cells (45,46), highly concentrated protein solutions have to be diluted before measurement. Therefore, the influence of protein concentration on $T_{m\ (nDSC)}$ could only be evaluated in the concentration range from 0.5 up to 5 mg/mL applicable for nDSC/μDSC. In Fig. 4, the excess heat capacity curves of the four proteins used including the thermal transition peaks are shown.

Table IV summarizes the thermodynamic results, where $T_{m\ (nDSC)}$ was defined as the peak maximum, the enthalpy change (ΔH_m) of the unfolding reaction at the melting temperature was obtained by integration of the area of the excess heat capacity endotherm, and the entropy difference (ΔS_m) was calculated by dividing ΔH_m by $T_{m\ (nDSC)}$. However, it should be mentioned that the maximum in the heat capacity (C_p) curves occurs near the $T_{m\ (nDSC)}$ and occurs directly at the $T_{m\ (nDSC)}$ only if $\Delta C_p = 0$, but this is typically only of marginal significance (42). The measured transition temperatures of all four proteins corresponded to the results known from literature. For example, BSA melted at a temperature of 63°C in a previous study (68), the melting temperature of an IgG_1 antibody was measured at 74°C (69), for β-LG, the $T_{m\ (nDSC)}$ was reported to be 87.6°C (70), and HEWL was described to be 50% denatured at a temperature of 76.1°C (71). Slight differences could be ascribed among other things to the protein quality used for nDSC/μDSC measurements, the solution conditions of the protein sample (e.g., pH, buffer system, addition of sodium chloride or other excipients), and the measurement parameters such as scanning rate applied.

Evidently, in this study, the calorimetric scans of BSA and the IgG_1 antibody revealed two unfolding endotherms: a main peak at 64°C with a smaller one exceeding 90°C or a primary peak at 73°C accompanied by a slight transition above 80°C, respectively. According to the results of Welfle *et al.* (72), the first peak in the biphasic IgG_1 antibody DSC curve might be attributed to the unfolding of the Fab fragment and the second peak to the Fc fragment of the monoclonal antibody. In terms of FTIR analysis, only one transition could be observed for these proteins. In contrast to the spectroscopic methods, one of the most important features of nDSC data is that the analysis does not require any assumption about the presence or absence of stable intermediates in the unfolding process. Furthermore, multistate transitions can be either detected directly or separated by a deconvolution algorithm (40,42). Nevertheless, the separate transition of the α-helix structure of β-LG occurring at a lower temperature in FTIR analysis compared to the changes in both the inter- and intramolecular β-sheet structures was not apparent in the calorimetric scans. In earlier calorimetric analysis, a shoulder of the main peak of lactoglobulin could be only identified at a very low scanning rate of 2°C/h (65). Hence, one could profit from FTIR analysis not only with regards to information about secondary structure changes but as well as with respect to the order in which these changes proceed. Considering the described examples of BSA, IgG_1, and β-LG, a combination of the two techniques used could yield better insight into the thermal unfolding behavior of the proteins.

Generally, a higher protein concentration leads to more symmetrical and narrower DSC peaks (73). This was particularly corroborated by the thermoscans of 0.5, 2, and 5 mg/mL BSA, β-LG, and HEWL. For β-LG, the melting temperatures varied markedly depending on the protein concentration as observed at 0.5 mg/mL β-LG, where the unfolding endotherm could not be detected because of a weak molar excess heat capacity resulting in a poor signal-to-noise ratio. For the other proteins, no impact of concentration on the $T_{m\ (nDSC)}$ value could be detected in the tested concentration range, although some converse examples are presented in literature. The unfolding temperature of IFN-β-1a declined from about 77 to 68°C, as the protein concentration was increased from 10 to 100 μg/mL (74). In spite of this, one has to consider that there is a huge difference between the concentration range applied in nDSC analysis in this study and the initial protein concentration of 100 mg/mL of highly concentrated formulations

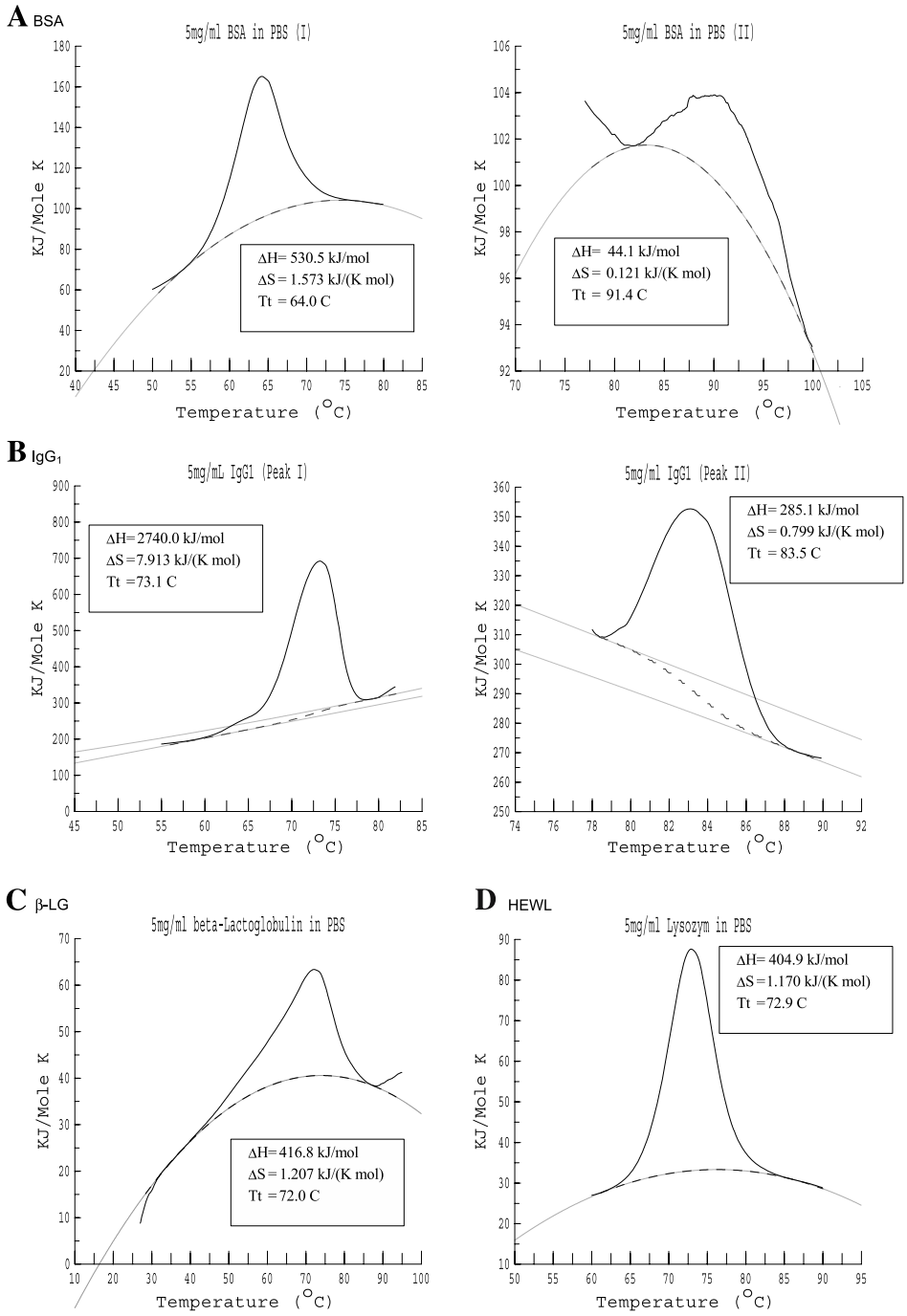

Fig. 4. Thermal transitions of (A) BSA, (B) IgG_1 antibody, (C) β-LG, and (D) HEWL each formulated at a concentration of 5 mg/mL in PBS, pH 7.2, as determined by nanodifferential scanning calorimetry.

before measurement. This may be crucial because high-concentration protein solutions are prone to protein interactions potentially leading to protein self-association and aggregation and therefore affecting the reversibility of the unfolding equilibrium. Consequently, the dilution of the high-concentration protein solutions before nDSC measurement is disadvantageous and contradicts the demand of maintaining the real conditions to potentially avoid analytical artifacts in order not to disturb protein's physical state.

In terms of the thermodynamic parameters (Table IV), the values of ΔH_m and ΔS_m increased in the following order: HEWL ≤ β-LG ≤ BSA < IgG_1 antibody, where, in the same order, the molecular weight rises. Robertson and Murphy (42) calculated values for the enthalpy as well as for the entropy change of the unfolding endotherm per unit surface area with dependency from apolar or polar residues, respectively, by a regression analysis of a database of 49 different proteins. The authors suggested that the primary determinant

Table IV. Thermodynamic Parameters ($T_{m\ (DSC)}$, ΔH, ΔS) of Four Proteins Obtained by nDSC Analysis with Dependency from Protein Concentration

Protein	Concentration (mg/mL)	Peak I			Peak II		
		$T_{m\ (nDSC)}$ (°C)	ΔH_m (kJ/mol)	ΔS_m (kJ/K mol)	$T_{m\ (nDSC)}$ (°C)	ΔH_m (kJ/mol)	ΔS_m (kJ/K mol)
BSA	0.5	63.4	285.5	0.85	n.a.[a]	n.a.[a]	n.a.[a]
	2	63.5	439.5	1.31	93.0	60.1	0.16
	5	64.0	530.5	1.57	91.4	44.1	0.12
IgG_1	0.5	72.9	2419.4	6.99	83.1	279.4	0.63
	2	72.8	2825.5	8.17	83.1	279.4	0.78
	5	73.1	2740.0	7.91	83.5	285.1	0.80
β-LG	0.5	n.a.[a]	n.a.[a]	n.a.[a]	n.a.[a]	n.a.[a]	n.a.[a]
	2	77.6	427.3	1.22	n.a.[a]	n.a.[a]	n.a.[a]
	5	72.0	416.8	1.21	n.a.[a]	n.a.[a]	n.a.[a]
HEWL	0.5	72.8	310.8	0.90	n.a.[a]	n.a.[a]	n.a.[a]
	2	72.8	367.7	1.06	n.a.[a]	n.a.[a]	n.a.[a]
	5	72.9	404.9	1.17	n.a.[a]	n.a.[a]	n.a.[a]

nDSC = nanodifferential scanning calorimetry.
[a] n.a. = not applicable or detectable.

of protein unfolding thermodynamics was the size of the protein. Whereas the enthalpy change of the unfolding endotherm results primarily from changes in solvation and noncovalent interactions, the entropy change upon unfolding includes additional contributions from changes in the configurational entropy of the side chains and the backbone. Besides the independence of $T_{m\ (nDSC)}$ values from protein concentration, the concentration seems to have no impact on the other thermodynamic parameters ΔH_m and ΔS_m. In the literature, an observed decrease in the enthalpy change was explained by the appearance of an aggregation process, which could lead to an exothermal peak and frequently could not be separated from the unfolding endotherms (75).

As mentioned in the previous section, the interpretation of thermodynamic parameters in terms of unfolding equilibria cannot be applied if reversibility of the unfolding reaction is not ensured. Thus, the use of the thermodynamic parameters would be feasible if reversibility of the unfolding reaction is checked by either performing a second scan on each protein or showing that the excess heat capacity curve is independent of the scan rate (40,42). However, if a system undergoes an irreversible process between two equilibrium states, one can still use an arbitrary reversible process to determine the enthalpy and entropy changes. This would be possible if the observed irreversibility of protein unfolding is caused by concomitant processes occurring significantly slower and with a significantly smaller enthalpy than the gross conformational changes (45). Typically, to achieve the mandatory reversible unfolding processes, it is compulsory that the proteins have to be fairly small (<30 kDa), dilute (<1 mg/mL), and highly charged to enhance electrostatic repulsion (67). The proteins used did not show any reversibility in unfolding under the conditions applied in this study because no endothermic peak was detectable during the second heating scan (data not shown). Thus, additional information about the enthalpic and entropic changes, being a potential added value of the calorimetric technique in comparison to FTIR analysis, could not be obtained for the high-concentration protein formulations.

A direct comparison of the consistent FTIR results of the IgG_1 antibody, which is primarily composed of intramolecular β-sheets as well as the clearly differing $T_{m\ (FTIR)}$ values of the α-helical protein HEWL with the transition temperatures obtained from nDSC technique, is given in Table V. For the IgG_1 antibody, the $T_{m\ (FTIR)}$ results determined as midpoint of the plot of the second-derivative

Table V. Comparison of the Transition Temperatures ($T_{m\ (FTIR)}$ *vs.* $T_{m\ (nDSC)}$) of the IgG_1 Antibody and HEWL with Dependency from Protein Concentration Obtained by FTIR and nDSC Analyses

Protein	Concentration (mg/mL)	$T_{m\ (FTIR)}$ (°C) Midpoints			$T_{m\ (nDSC)}$ (°C)
		Method i: increasing band (second derivation)	Method ii: decreasing band (second derivation)	Method iii: ratio of increasing to decreasing band	Peak I
IgG_1	2	n.d.[a]	n.d.[a]	n.d.[a]	72.8
	5	74.3 ± 0.2	76.3 ± 0.5	73.8 ± 0.3	73.1
	100	74.7 ± 0.1	76.1± 0.3	74.3 ± 0.2	n.d.[a]
HEWL	2	n.d.[a]	n.d.[a]	n.d.[a]	72.8
	5	79.5 ± 0.3	61.1 ± 0.9	79.1 ± 0.3	72.9
	100	74.3 ± 0.5	78.6 ± 0.2	75.3 ± 0.3	n.d.[a]

[a] n.d. = not determined.

Table VI. Comparison of the Two Analytical Methods FTIR and nDSC with Respect to Their use for the Measurement of Transition Temperatures

Criterion	FTIR	nDSC
Material requirements	Low (15 μL)	High (>1 mL)
Concentration range	≥2 mg/mL	Approx. 0.5–5 mg/mL
Heating rate	Not defined	Defined
	Interruption of temperature ramp during the measurement	Linear
Additional information	Changes in secondary structure (possibly detection of order of unfolding of different structural elements)	Thermodynamic parameters (C_p, ΔH, ΔS)
	Appearance of precipitation	Detection of intermediates by deconvolution algorithms
	Reversibility of unfolding	Reversibility of unfolding

intensity of the arising intermolecular β-sheets *vs.* temperature as well as of the curve of the ratio of the unmodified intensities of the structural loss to the temperature-induced structural element matched the melting temperature of the nDSC thermoscans very well (difference ≤2°C). Slight variations in the T_m values comparing μDSC/nDSC and FTIR analysis have been also mentioned by other authors. For instance, the $T_{m\ (FTIR)}$ values determined for recombinant human interferon-γ as a midpoint of the intensity–temperature plots of second-derivative infrared bands assignable to α-helix or intermolecular β-sheet frequencies differ in a range of about 2°C from the DSC result (63). Small differences could be explained by the fact that the heating rates of the calorimeter do not match the infrared analysis because of the necessity of averaging of spectral data at each temperature step to obtain a sufficient signal-to-noise ratio. Whereas the temperature profile applied for the nDSC measurements was completely linear, the increase in temperature during FTIR analysis was interrupted at each scanning point for approximately 2 min. For the α-helical protein HEWL, only the FTIR data interpretation method using the midpoint of the second-derivative intensity–temperature curve (because of the intermolecular β-sheet mode) could be applied because this data interpretation technique resulted in the closest agreement with the nDSC technique. In this case, the results obtained from FTIR were consistent with the transition temperatures of the nDSC thermograms only if the FTIR measurement had been performed at a concentration of 100 mg/mL. Therefore, it is recommended to utilize the temperature curves of the second-derivative intensities of the arising β-aggregates (method i) and to perform FTIR measurements at high protein concentrations. To appraise the pros and cons of the two analytical methods FTIR and nDSC discussed so far, Table VI offers a summary of the favorable and disadvantageous features regarding T_m analysis.

However, the following question arises: does the transition temperature resulting from calorimetric or spectral analysis really give insight into the conformational stability of the protein? The conformational stability of the folded state of the protein is defined as the difference in Gibbs free energy change ΔG_u between the denatured state and the native state

$$\Delta G_u(T) = \Delta H_u(T) - T\Delta S_u(T) \quad (1)$$

where ΔH_u and ΔS_u are the differences in the enthalpy and entropy at the same temperature at which ΔG_u is being evaluated, respectively (38,42). Hence, the difference in Gibbs energy ΔG as a function of temperature needs to be related to the melting temperature (T_m). This can be achieved by the modified Gibbs-Helmholtz equation

$$\Delta G(T) = \Delta H_m\left(1 - \frac{T}{T_m}\right) - \Delta C_p\left[(T_m - T) + T\ln\left(\frac{T}{T_m}\right)\right] \quad (2)$$

which links the difference in Gibbs energy as a function of temperature to the enthalpy of unfolding (ΔH_m) and the heat capacity change between the folded and unfolded state (ΔC_p), measured at T_m, and allows calculation of ΔG for each temperature (40,42). Plotting ΔG *vs.* temperature shows that a protein is stable over a wide temperature range where the free energy of unfolding is positive. At the temperature of maximal stability (T_s), generally around 20°C, the entropy of protein unfolding is zero, and the protein is stabilized solely by the enthalpy term. At temperatures below or above T_s, the free energy change declines, whereby zero stability (i.e., $\Delta G = 0$) is attained at two different transition temperatures. This is, on one hand, the melting temperature of the heat denaturation reaction measured by nDSC and FTIR in this study. On the other hand, a second transition temperature exists at which cold triggers the breakdown of the native structure. Whereas heat denaturation is induced by the gain of conformational entropy, an increase of the solvation tendency caused by hydration of apolar groups leads to the denaturation at lower temperatures (38,46,76). The larger the value of ΔG, the more stable is the protein, albeit it ranges usually from 5 to 60 kcal/mol, indicating that the folded state is only marginally more stable than the unfolded state (77). Consecutively, there is no particular relationship between T_m and protein stability as measured by ΔG (78). Yet, a higher transition temperature is often associated with greater thermal resistance of a protein, which implies that a high T_m value ensures the best chance of stability at lower temperature ranges despite the fact that some well-known exceptions exist (4,40,78).

CONCLUSIONS

Summing up the results of this study, determination of a $T_{m\ (FTIR)}$ is feasible by calculation of the midpoint of a

sigmoidal curve originating from the intensity–temperature plot of the arising intermolecular β-sheet band. However, more significant results were obtained for proteins that are predominantly composed of intramolecular β-sheets and where FTIR measurements are performed at higher protein concentrations. Moreover, FTIR is preferred over nDSC for analysis of high-concentration protein formulations because the protein can be measured without prior dilution, i.e., at real solution conditions without the fear of artificial changes in the protein's physical state. Additionally, the benefit of material savings in FTIR analysis as compared to nDSC technique is particularly valuable in the development of high-concentration protein solutions.

However, the FTIR technique should be evaluated with regard to its applicability in formulation development and the predictability of protein stability in high-concentration formulations by $T_{m\ (FTIR)}$ values. In a second study, FTIR analysis will be investigated to support the formulation development of a high-concentration IgG_1 antibody formulation.

ACKNOWLEDGMENTS

The authors thank Claudia Borst and Franziska Huber for their assistance in the experimental work.

REFERENCES

1. A. K. Pavlou and M. J. Belsey. The therapeutic antibodies market to 200. *Eur. J. Pharm. Biopharm.* **59**:389–396 (2005).
2. S. J. Shire, Z. Shakrokh, and J. Liu. Challenges in the development of high protein concentration formulations. *J. Pharm. Sci.* **93**:1390–1402 (2004).
3. J. L. Cleland, M. F. Powell, and S. J. Shire. The development of stable protein formulations: a close look at protein aggregation, deamidation, and oxidation. *Crit. Rev. Ther. Drug Carr. Syst.* **10**:307–377 (1993).
4. M. C. Manning, K. Patel, and R. T. Borchardt. Stability of protein pharmaceuticals. *Pharm. Res.* **6**:903–918 (1989).
5. W. Wang. Instability, stabilization, and formulation of liquid protein pharmaceuticals. *Int. J. Pharm.* **185**:129–188 (1999).
6. W. Wang. Protein aggregation and its inhibition in biopharmaceutics. *Int. J. Pharm.* **289**:1–30 (2005).
7. R. Harris, S. J. Shire, and C. Winter. Commercial manufacturing scale formulation and analytical characterization of therapeutic recombinant antibodies. *Drug Dev. Res.* **61**:137–154 (2004).
8. S. Y. Patro, E. Freund, and B. S. Chang. Protein formulation and fill-finish operations. *Biotechnol. Annu. Rev.* **8**:55–84 (2002).
9. V. N. Uversky, J. Li, and A. L. Fink. Evidence for a partially folded intermediate in alpha-synuclein fibril formation. *J. Biol. Chem.* **276**:10737–10744 (2001).
10. D. B. Volkin, G. Sanyal, C. J. Burke and C. R. Middaugh. Preformulation studies as an essential guide to formulation development and manufacture of protein pharmaceuticals. In S. L. Nail and M. J. Akers (eds.), *Development and Manufacture of Protein Pharmaceuticals*, Kluwer Academic/Plenum Publishers, New York, 2002, pp. 1–46.
11. C. N. Pace, B. A. Shirley, and J. A. Thomson. Measuring the conformational stability of a protein. In: Protein Structure, 1989, pp. 311–330.
12. J. T. Pelton and L. R. McLean. Spectroscopic methods for analysis of protein secondary structure. *Anal. Biochem.* **277**: 167–176 (2000).
13. E. A. Cooper and K. Knutson. Fourier transform infrared spectroscopy investigations of protein structure. In J. N. Herron, W. Jiskoot, and D. J. Crommelin (eds.), *Physical Methods to Characterize Pharmaceutical Proteins*, Plenum Press, New York, 1995, p101.
14. W. Surewicz, H. Mantsch, and D. Chapmann. Determination of protein secondary structure by Fourier transform infrared spectroscopy: A critical assessment. *Biochemistry* **32**:389–394 (1993).
15. J. F. Carpenter and J. H. Crowe. An infrared spectroscopic study of the interactions of carbohydrates with dried proteins. *Biochemistry* **28**:3916–3922 (1989).
16. J. F. Carpenter, S. J. Prestrelski, and A. Dong. Application of infrared spectroscopy to development of stable lyophilized protein formulations. *Eur. J. Pharm. Biopharm.* **45**:231–238 (1998).
17. H. R. Costantino, K. Griebenow, P. Mishra, R. Langer, and A. M. Klibanov. Fourier-transform infrared spectroscopic investigation of protein stability in the lyophilized form. *Biochim. Biophys. Acta* **1253**:69–74 (1995).
18. A. Dong, S. J. Prestrelski, S. D. Allison, and J. F. Carpenter. Infrared spectroscopic studies of lyophilization- and temperature-induced protein aggregation. *J. Pharm. Sci.* **84**:415–424 (1995).
19. K. Griebenow and A. M. Klibanov. Lyophilization-induced reversible changes in the secondary structure of proteins. *Proc. Natl. Acad. Sci. USA* **92**:10969–10976 (1995).
20. S. J. Prestrelski, K. A. Pikal, and T. Arakawa. Optimization of lyophilization conditions for recombinant human interleukin-2 by dried-state conformational analysis using Fourier-transform infrared spectroscopy. *Pharm. Res.* **12**:1250–1259 (1995).
21. S. J. Prestrelski, N. Tedeschi, T. Arakawa, and J. F. Carpenter. Dehydration-induced conformational transitions in proteins and their inhibition by stabilizers. *Biophys. J.* **65**:661–671 (1993).
22. M. Maury, K. Murphy, S. Kumar, A. Mauerer, and G. Lee. Spray-drying of proteins: effects of sorbitol and trehalose on aggregation and FT-IR amide I spectrum of an immunoglobulin G. *Eur. J. Pharm. Biopharm.* **59**:251–261 (2005).
23. S. Schüle, T. Schultz-Fadenrecht, S. Bassarab, K. Bechtold-Peters, W. Friess, and P. Garidel. Determination of the secondary protein structure of IgG1 antibody formulations for spray drying. *Respir. Drug Deliv.* **IX**:377–380 (2004).
24. J. Wang, K. M. Chua, and C. H. Wang. Stabilization and encapsulation of human immunoglobulin G into biodegradable microspheres. *J. Colloid Interface Sci.* **271**:92–101 (2004).
25. A. Wittemann and M. Ballauff. Secondary structure analysis of proteins embedded in spherical polyelectrolyte brushes by FT-IR spectroscopy. *Anal. Chem.* **76**:2813–2819 (2004).
26. C. M. Dobson. Experimental investigation of protein folding and misfolding. *Methods* **34**:4–14 (2004).
27. A. Dong, B. F. Kendrick, L. Kreilgard, J. Matsuura, M. C. Manning, and J. F. Carpenter. Spectroscopic study of secondary structure and thermal denaturation of recombinant human factor XIII in aqueous solution. *Arch. Biochem. Biophys.* **347**:213–220 (1997).
28. R. Moritz, D. Reinstädler, H. Fabian, and D. Naumann. Time-resolved FTIR difference spectroscopy as tool for investigating refolding reactions of ribonuclease T1 synchronized with trans cis prolyl isomerization. *Biopolymers (Biospectroscopy)* **67**: 145–155 (2002).
29. N. Takeda, M. Kato, and Y. Taniguchi. Pressure- and thermally-induced reversible changes in the secondary structure of ribonuclease A studied by FT-IR spectroscopy. *Biochemistry* **34**:5980–5987 (1995).
30. A. Dong, T. W. Randolph, and J. F. Carpenter. Entrapping intermediates of thermal aggregation in alpha-helical proteins with low concentration of guanidine hydrochloride. *J. Biol. Chem.* **275**:27689–27693 (2000).
31. A. A. Ismail, H. H. Mantsch, and P. T. Wong. Aggregation of chymotrypsinogen: portrait by infrared spectroscopy. *Biochim. Biophys. Acta* **1121**:183–188 (1992).
32. V. Militello, C. Casarino, A. Emanuele, A. Giostra, F. Pullara, and M. Leone. Aggregation kinetics of bovine serum albumin

studied by FTIR spectroscopy and light scattering. *Biophys. Chem.* **107**:175–187 (2004).
33. J. L. R. Arrondo, A. Muga, J. Castresana, and F. M. Goni. Quantitative studies of the structure of proteins in solution by Fourier-transform infrared spectroscopy. *Prog. Biophys. Mol. Biol.* **59**:23–56 (1993).
34. A. Dong, J. Matsuura, S. D. Allison, E. Chrisman, M. C. Manning, and J. F. Carpenter. Infrared and circular dichroism spectroscopic characterization of structural differences between β-lactoglobulin A and B. *Biochemistry* **35**:1450–1457 (1996).
35. R. Krishnamurthy and M. C. Manning. The stability factor: Importance in formulation development. *Curr. Pharm. Biotechnol.* **3**:361–371 (2002).
36. D. B. Volkin and C. R. Middaugh. The effect of temperature on protein structure. In T. J. Ahern and M. C. Manning (eds.), *Stability of Protein Pharmaceuticals, Part A: Chemical and Physical Pathways of Protein Degradation*, Plenum Press, New York, 2003, pp. 215–247.
37. B. F. Kendrick, A. Dong, S. D. Allison, M. C. Manning, and J. F. Carpenter. Quantitation of the area of overlap between second-derivative amide I infrared spectra to determine the structural similarity of a protein in different states. *J. Pharm. Sci.* **85**: 155–158 (1996).
38. M. van de Weert, P. I. Haris, W. E. Hennink, and D. J. A. Crommelin. Fourier transform infrared spectrometric analysis of protein conformation: effect of sampling method and stress factors. *Anal. Biochem.* **297**:160–169 (2001).
39. W. J. Becktel and J. A. Schellmann. Protein stability curves. *Biopolymers* **26**:1859–1877 (1987).
40. M. Cauchy, S. D'Aoust, B. Dawson, H. Rode, and M. A. Hefford. Thermal stability: a means to assure tertiary structure in therapeutic proteins. *Biologicals* **30**:175–185 (2002).
41. R. L. Remmele Jr. and W. R. Gombotz. Differential scanning calorimetry: a practical tool for elucidating the stability of liquid biopharmaceuticals. *Biopharm. Europe* **13**:56–65 (2000).
42. P. M. Bummer and S. Koppenol. Chemical and physical considerations in protein and peptide stability. In E. J. McNally (ed.), *Protein Formulation and Delivery*, Marcel Dekker Inc., New York, 2000, pp. 5–69.
43. A. D. Robertson and K. P. Murphy. Protein structure and the energetics of protein stability. *Chem. Rev.* **97**:1251–1267 (1997).
44. T. Chen and D. M. Oakley. Thermal analysis of proteins of pharmaceutical interest. *Thermochim Acta* **248**:229–244 (1995).
45. V. L. Shnyrov, J. M. Sanchez-Ruiz, B. N. Boiko, G. Zhadan, and E. A. Permyakov. Applications of scanning microcalorimetry in biophysics and biochemistry. *Thermochim. Acta* **302**:165–180 (1997).
46. P. L. Privalov and S. A. Potekhin. Scanning microcalorimetry in studying temperature-induced changes in proteins. *Methods Enzymol.* **131**:4–50 (1986).
47. P. L. Privalov. Thermodynamic problems of protein structure. *Annu. Rev. Biophys. Biomol. Struct.* **18**:47–69 (1989).
48. A. Savitzky and M. J. E. Golay. Smoothing and differentiation of data by simplified least squares procedures. *Anal. Chem.* **36**:1627–1639 (1964).
49. W. Surewicz and H. Mantsch. New insight into protein secondary structure from resolution-enhanced infrared spectra. *Biochim. Biophys. Acta* **952**:115–130 (1988).
50. T. Maruyama, S. Katoh, M. Nakajima, and H. Nabetani. Mechanism of bovine serum albumin aggregation during ultrafiltration. *Biotechnol. Bioeng.* **75**:233–238 (2001).
51. K. Murayama and M. Tomida. Heat-induced secondary structure and conformation change of bovine serum albumin investigated by Fourier transform infrared spectroscopy. *Biochemistry* **43**:11526–11532 (2004).
52. J. Zhang and Y. B. Yan. Probing conformational changes of proteins by quantitative second-derivative infrared spectroscopy. *Anal. Biochem.* **340**:89–98 (2005).
53. H. R. Costantino, J. D. Andya, S. J. Shire, and C. C. Hsu. Fourier-transform infrared spectroscopic analysis of the secondary structure of recombinant humanized immunoglobulin G. *Pharm. Sci.* **3**:121–128 (1997).
54. M. Levitt and J. Greer. Automatic identification of secondary structure in globular proteins. *J. Mol. Biol.* **114**:181–239 (1977).
55. A. Bhattacharjee, S. Saha, A. Biswas, M. Kundu, L. Ghosh, and K. P. Das. Structural changes of beta-lactoglobulin during thermal unfolding and refolding—An FT-IR and circular dichroism study. *Protein J.* **24**:27–35 (2005).
56. G. Panick, R. Malessa, and R. Winter. Differences between the pressure- and temperature-induced denaturation and aggregation of -lactoglobulin A, B, and AB monitored by FT-IR spectroscopy and small-angle X-ray scattering. *Biochemistry* **38**:6512–6519 (1999).
57. D. M. Byler and H. Susi. Examination of the secondary structure of proteins by deconvolved FT-IR. *Biopolymers* **25**:469–487 (1986).
58. X. L. Qi, C. Holt, D. McNulty, D. T. Clarke, S. Brownlow, and G. R. Jones. Effect of temperature on the secondary structure of b-lactoglobulin at pH 6.7, as determined by CD and IR spectroscopy: a test of the molten globule hypothesis. *Biochem. J.* **324**:341–346 (1997).
59. Y.-H. Liao, M. B. Brown, T. Nazir, A. Quader, and G. P. Martin. Effect of sucrose and trehalose on the preservation of the native structure of spray-dried lysozyme. *Pharm. Res.* **19**:1847–1853 (2002).
60. J. F. Carpenter, B. S. Kendrick, B. S. Chang, M. C. Manning, and T. W. Randolph. Inhibition of stress-induced aggregation of protein therapeutics. *Methods Enzymol.* **309**:236–255 (1999).
61. A. S. Lee, C. Galea, E. L. DiGiammarino, B. Jun, G. Murti, R. C. Ribeiro, G. Zambetti, C. P. Schultz, and R. W. Kriwacki. Reversible amyloid formation by the p53 tetramerization domain and a cancer-associated mutant. *J. Mol. Biol.* **327**:699–709 (2003).
62. E. Querol, J. A. Perez-Pons, and A. Mozo-Villarias. Analysis of protein conformational characteristics related to thermostability. *Protein Eng.* **9**:265–271 (1996).
63. B. S. Kendrick, J. L. Cleland, X. M. Lam, T. Nguyen, T. W. Randolph, M. C. Manning, and J. F. Carpenter. Aggregation of recombinant human interferon gamma: kinetics and structural transitions. *J. Pharm. Sci.* **87**:1069–1076 (1998).
64. A. Muga, H. H. Mantsch, and W. Surewicz. Membrane binding induces destabilization of cytochrome *c* structure. *Biochemistry* **30**:7219–7224 (1991).
65. M. A. M. Hoffmann, J. C. van Miltenburg, and P. J. J. M. van Mil. The suitability of scanning calorimetry to investigate slow irreversible protein denaturation. *Thermochim. Acta* **306**: (1997).
66. B. A. Shirley. Protein conformational stability estimated from urea, guanidine hydrochloride, and thermal denaturation curves. In T. J. Ahern and M. C. Manning (eds.), *Stability of Protein Pharmaceuticals, Part A: Chemical and Physical Pathways of Protein Degradation*, Plenum Press, New York, 1992, pp. 167–194.
67. B. S. Kendrick, T. Li, and B. S. Chang. Physical stabilization of proteins in aqueous solution. In J. F. Carpenter and M. C. Manning (eds.), *Rational Design of Stable Protein Formulations: Theory and Practice*, Kluwer Academic/Plenum Publishers, New York, 2003, pp. 61–84.
68. M. Yamasaki, H. Yano, and K. Aoki. Differential scanning calorimetric studies on bovine serum albumin: I. effects of pH and ionic strength. *Int. J. Biol. Macromol.* **12**:263–268 (1990).
69. A. W. P. Vermeer, M. G. E. G. Bremer, and W. Norde. Structural changes of IgG induced by heat treatment and by adsorption onto a hydrophobic Teflon surface studied by circular dichroism spectroscopy. *Biochim. Biophys. Acta (G)* **1425**:1–12 (1998).
70. P. Relkin, L. Eynard, and B. Launay. Thermodynamic parameters of [beta]-lactoglobulin and [alpha]-lactalbumin. A DSC study of denaturation by heating. *Thermochim. Acta* **204**: 111–121 (1992).
71. A. A. Elkordy, R. T. Forbes, and B. W. Barry. Stability of crystallised and spray-dried lysozyme. *Int. J. Pharm.* **278**:209–219 (2004).
72. K. Welfle, R. Misselwitz, G. Hausdorf, W. Hohne, and H. Welfle. Conformation, pH-induced conformational changes, and thermal unfolding of anti-p24 (HIV-1) monoclonal antibody CB4-1 and its Fab and Fc fragments. *Biochim. Biophys. Acta, Prot. Struct. Mol. Enzymol.* **1431**:120–131 (1999).
73. X. L. Qi, S. Brownlow, C. Holt, and P. Sellers. Thermal denaturation of [beta]-lactoglobulin: effect of protein concen-

tration at pH 6.75 and 8.05. *Biochim. Biophys. Acta, Prot. Struct. Mol. Enzymol.* **1248**:43–49 (1995).
74. L. Runkel, W. Meier, R. B. Pepinsky, M. Karpusas, A. Whitty, K. Kimball, M. Brickelmaier, C. Muldowney, W. Jones, and S. E. Goelz. Structural and functional differences between glycosylated and non-glycosylated forms of human interferon-γ (IFN-γ). *Pharm. Res.* **15**:641–649 (1998).
75. M. Cueto, M. J. Dorta, O. Munguia, and M. Llabrés. New approach to stability assessment of protein solution formulations by differential scanning calorimetry. *Int. J. Pharm.* **252**:159–166 (2003).
76. P. L. Privalov and S. J. Gill. Stability of protein structure and hydrophobic interaction. *Adv. Protein Chem.* **39**:191–234 (1988).
77. Y.-C. J. Wang and M. A. Hanson. Parenteral formulations of proteins and peptides: stability and stabilizers. *PDA J. Pharm. Sci. Technol.* **42**:S1–S25 (1988).
78. K. A. Dill, D. O. Alonso, and K. Hutchinson. Thermal stabilities of globular proteins. *Biochemistry* **28**:5439–5449 (1989).